AEROSOL ATTENUATION IN THE 2-4 MICROMETER REGION

Robert C. Sepucha, et al

Aerodyne Research, Incorporated

Prepared for:

Rome Air Development Center
Defense Advanced Research Projects Agency

March 1975

RADC-TR-75-113
Technical Report
March 1975

AEROSOL ATTENUATION IN THE 2-4 μm REGION

Aerodyne Research, Inc.

Sponsored By
Defense Advanced Research Projects Agency
ARPA Order No. 1279

Approved for public release;
distribution unlimited.

The views and conclusions contained in this document are those of the authors and should not be interpreted as necessarily representing the official policies, either expressed or implied, of the Defense Advanced Research Projects Agency or the U. S. Government.

Rome Air Development Center
Air Force Systems Command
Griffiss Air Force Base, New York 13441

UNCLASSIFIED

SECURITY CLASSIFICATION OF THIS PAGE (When Data Entered)

REPORT DOCUMENTATION PAGE		READ INSTRUCTIONS BEFORE COMPLETING FORM
1. REPORT NUMBER RADC-TR-75-113	2. GOVT ACCESSION NO.	3. RECIPIENT'S CATALOG NUMBER
4. TITLE (and Subtitle) AEROSOL ATTENUATION IN THE 2-4 μm REGION		5. TYPE OF REPORT & PERIOD COVERED Semiannual Report 20 May 74 - 20 Nov 74
		6. PERFORMING ORG. REPORT NUMBER ARI - RR - 58
7. AUTHOR(s) Dr. Robert C. Sepucha Dr. David C. Mann		8. CONTRACT OR GRANT NUMBER(s) F30602-74-C-0282
9. PERFORMING ORGANIZATION NAME AND ADDRESS Aerodyne Research, Inc. 20 South Avenue Burlington, Ma 01803		10. PROGRAM ELEMENT, PROJECT, TASK AREA & WORK UNIT NUMBERS P. E. 62301E J. O. 12790505
11. CONTROLLING OFFICE NAME AND ADDRESS Defense Advanced Research Projects Agency 1400 Wilson Blvd Arlington VA 22209		12. REPORT DATE March 1975
		13. NUMBER OF PAGES 43
14. MONITORING AGENCY NAME & ADDRESS (if different from Controlling Office) Rome Air Development Center (OCSE) Griffiss AFB NY 13441		15. SECURITY CLASS. (of this report) UNCLASSIFIED
		15a. DECLASSIFICATION/DOWNGRADING SCHEDULE N/A

16. DISTRIBUTION STATEMENT (of this Report)

Approved for public release; distribution unlimited.

17. DISTRIBUTION STATEMENT (of the abstract entered in Block 20, if different from Report)

Same

18. SUPPLEMENTARY NOTES

RADC Project Engineer:
James W. Cusack (OCSE)
AC 315 330-3145

19. KEY WORDS (Continue on reverse side if necessary and identify by block number)

Aerosol
DF Laser
Aerosol Infrared Absorption
Aerosol Infrared Extinction
White Cell

20. ABSTRACT (Continue on reverse side if necessary and identify by block number)

This report describes an experimental facility being constructed to measure the extinction and scattering of DF laser radiation by atmospheric aerosols. The details of the apparatus and the theory of the measurements are presented.

DD FORM 1 JAN 73 1473 EDITION OF 1 NOV 65 IS OBSOLETE

UNCLASSIFIED PRICES SUBJECT TO CHANGE

SECURITY CLASSIFICATION OF THIS PAGE (When Data Entered)

AEROSOL ATTENUATION IN THE 2-4 μm REGION

Dr. Robert C. Sepucha
Dr. David Mann

Contractor: Aerodyne Research, Inc.
Contract Number: F30602-74-C-0282
Effective Date of Contract: 20 May 1974
Contract Expiration Date: 15 August 1975
Amount of Contract: $174,250.00
Program Code Number: 5E20
Period Covered: 20 May 74 - 20 Nov 74

Principal Investigator: Dr. Robert C. Sepucha
Phone: 617 272-1100
Dr. David Mann
Phone: 617 272-1100

Project Engineer: James W. Cusack
Phone: 315 330-3145

Approved for public release;
distribution unlimited.

This research was supported by the Defense Advanced Research Projects Agency of the Department of Defense and was monitored by James W. Cusack RADC (OCSE), GAFB NY 13441 under Contract F30602-74-C-0282, Job Order No. 12790505.

This report has been reviewed by the RADC Information Office (OI) and is releasable to the National Technical Information Service (NTIS). At NTIS it will be releasable to the general public, including foreign nations.

This technical report has been reviewed and approved for publication.

APPROVED: 

RADC Project Engineer

TABLE OF CONTENTS

LIST OF ILLUSTRATIONS

1. INTRODUCTION

1.1 Program Objectives

The experimental program described in this semiannual report is designed to obtain data on the fundamental optical properties of atmospheric aerosols at DF laser wavelengths in the 2 to 4 μm spectral region.

Atmospheric attenuation of DF laser radiation is not well defined at present. The 3 to 4 μm region is considered to be an atmospheric window because of relatively low molecular absorption. However, aerosol extinction has been estimated to be comparable to or greater than molecular absorption in this region. Unfortunately the scarcity of data on aerosol optical properties makes these estimates unreliable for systems evaluation, although both scattering and absorption contribute to laser attenuation. It is absorption which affects the onset of such deleterious effects as thermal blooming. Since the threshold for aerosol induced thermal blooming is a function of the aerosol absorption coefficient at the particular wavelength of interest, there is particular interest in the degree of aerosol absorption at DF laser wavelengths.

The program described in this report and currently underway at Aerodyne Research, Inc., is designed to measure the total extinction (scattering plus absorption) and the scattering of DF laser radiation by atmospheric aerosols. The data will yield directly the corresponding extinction and scattering coefficients, the difference of which is the desired absorption coefficient. Such data will permit an accurate assessment of the role of aerosols in atmospheric attenuation and in degradation of DF laser beam profiles.

An integral part of the program is an extensive effort to characterize the atmospheric aerosols used in the measurements. The aerosols will be characterized by their chemical composition, particle number density and mass loading. This will provide a means of relating the optical data obtained in this program to aerosols found in other geographic areas.

1.2 Technical Approach and Report Summary

The scope of the program includes the design and fabrication of the experimental facilities necessary for the measurement of the aerosol extinction and scattering coefficients as well as the collection and analysis of data to determine the aerosol absorption coefficient at DF laser wavelengths.

The extinction and scattering measurements will be performed on ambient aerosols sampled at Aerodyne Research, Inc. in Burlington, Massacusetts. Aerosol-laden air will be drawn into the experimental apparatus from a point 10 ft above the roof of the building. A continuously flowing system will circulate the air through a scattering cell and through a folded-path White cell where the extinction measurements will be made. The White cell has been specifically designed and fabricated for this program. Its design includes the unique feature of aerodynamic windows which protect the optical elements in the cell from contamination by the aerosol.

The output beam from a pulsed DF laser will be split and directed into both cells. Infrared detection systems will then permit simultaneous measurement of the absolute scattered intensity and the extinction produced by the aerosol.

The aerosol handling system will be equipped with filters which will collect the aerosol particles. These samples will be subjected to an elemental chemical analysis performed by an outside laboratory. A commerical particle counter will be used to determine the particle number density. The temperature and relative humidity will be monitored continuously, both inside the apparatus and on the roof where the aerosol is drawn into the building.

At present, the fabrication and assembly of the experimental apparatus are nearing completion. Component testing and calibration are scheduled to begin shortly.

The details of the experimental facility are presented in Section 2 of this report. The theory of the measurement and the equipment designed to perform the measurement are described for both extinction and scattering. Calibration procedures, measurement sensitivity, and accuracy are described. Finally, a description of the aerosol characterization aspect of the program is presented. Section 2 concludes with Subsection 2.6 which summarizes the present status of the program and the schedule of work for the following reporting period.

2. EXPERIMENTAL INVESTIGATION

2.1 Introduction

The primary objective of the experimental program as described in Section 1 is to determine the absorption coefficient of ambient atmospheric aerosols at DF laser wavelengths. Since the absorption cannot be measured directly, both the aerosol extinction coefficient (absorption plus scattering) and the scattering coefficient will be measured simultaneously, and the difference of the two will be taken to obtain the desired result. In the present section, we present a detailed discussion of the theory of the measurements and the apparatus required to obtain the data. In addition, calibration procedures and predicted measurement sensitivity are given for each measurement. The extinction measurement is described in Subsection 2.2, and the scattering measurement is discussed in Subsection 2.3.

2.2 Extinction Measurement

2.2.1 Theory of the Measurement

The extinction coefficient for atmospheric aerosols will be determined by measuring the attenuation of DF laser radiation as it propagates through a folded-path geometry for a total distance of up to 400m. In this part of the subsection, we describe the theory of the measurements, and the method by which the extinction coefficient, k_{ext}, is determined from the laboratory data. The experimental apparatus, the calibration techniques, and an error analysis are discussed in the succeeding parts of Subsection 2.2.

The laboratory apparatus is shown schematically in Figure 2.1. The single-line, diffraction-limited output from a DF TEA laser is focused onto the entrance plane of a 400m White cell. Eighty traversals of a 5m path are used to obtain the total-path length. After passing through the aerosol in the cell, the emerging beam of intensity I is focused onto infrared detector D_4, and produces a voltage V. Ahead of the White cell, the laser beam is sampled with a beam splitter. The reference beam of intensity I_o is focused onto a second detector D_3, and produces a voltage V_o.

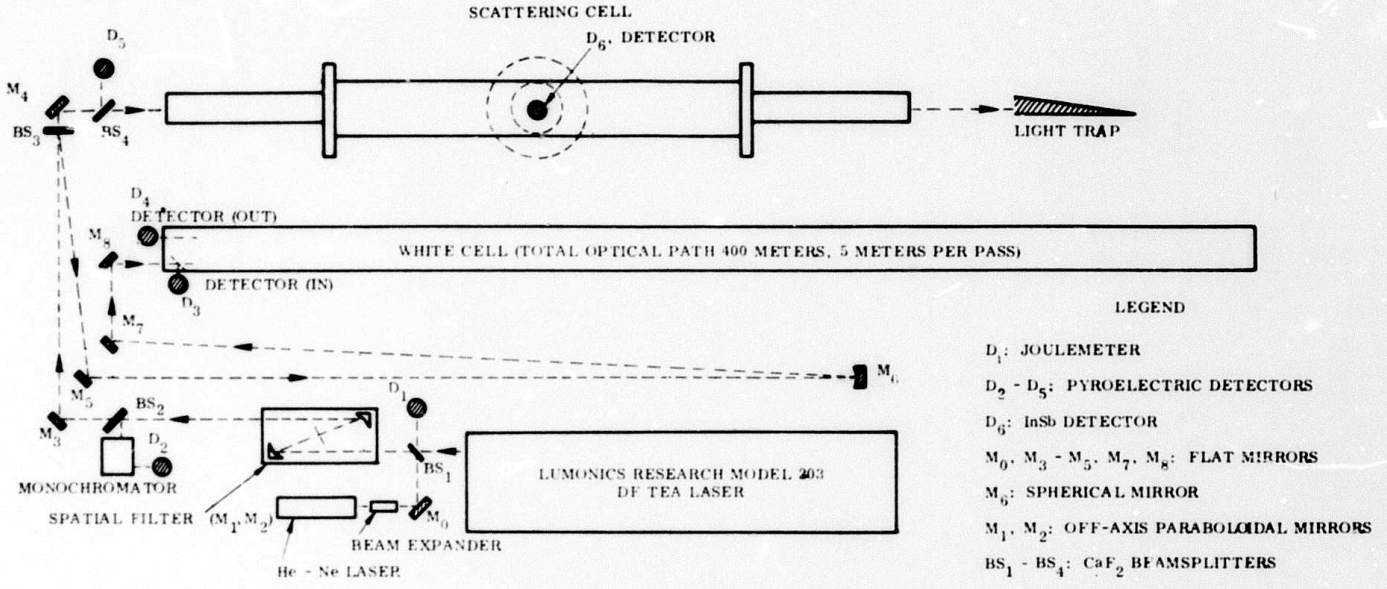

Figure 2.1 - Schematic of Experimental Apparatus.

For every microsecond laser pulse, two quantities will be measured: the reference intensity I_o and the intensity difference $(I_o - I)$. The extinction coefficient follows from Beer's law

$$I = I_o \exp(-k_{ext} L) \tag{2.1}$$

This relationship assumes that energy is lost from the beam only by first-order processes such as single absorption and scattering, and not by higher-order effects such as multiple scattering. Single scattering prevails so long as $k_{ext} L < 0.1$. For naturally occurring aerosols, the upper bound on the expected extinction coefficient is $10^{-1} km^{-1}$. Thus $k_{ext} L$ will be, at most, about 10^{-2} in the experiments.

For such small values, it is advantageous to expand the exponential in a power series,

$$\exp(-k_{ext} L) = 1 - k_{ext} L + \frac{(k_{ext} L)^2}{2} - \frac{(k_{ext} L)^3}{3} + \ldots.$$

Retaining the first three terms and rearranging Eq. (2.1) yields

$$\frac{(I_o - I)}{I_o} \simeq k_{ext} L - \frac{(k_{ext} L)^2}{2} \quad . \tag{2.2}$$

For values of $k_{ext} L$ on the order of 10^{-2}, this approximation introduces an error on the order of 10^{-4}. Equation (2.2) forms the basis for determining $k_{ext} L$ in very weakly attenuating systems.

In the experimental arrangement shown in Figure 2.1, the reference signal V_o is set equal to the signal V in the absence of an attenuating medium in the White cell, in which case the output of the differential amplifier is zero, aside from a noise component due to detector-plus-amplifier noise. With an attenuating medium in the White cell, the signal V_o is greater than V, and the differential amplifier output becomes $V_o - V$.

To determine the aerosol extinction, the difference measurements will be made in the following three situations: when the absorption cell is (1) empty, (2) filled with filtered air, and (3) filled with aerosol-ladened air. This will supply a reference of zero-attenuation, attenuation due to molecular absorption, and attenuation due to molecular absorption and aerosol extinction. In this way, the molecular contribution can be subtracted from the attenuation, leaving only the aerosol contribution.

An alternate method would employ several laser lines. Assuming the aerosol contribution is the same for all lines, one can subtract out the molecular contribution from the total extinction, leaving the contribution due to aerosol extinction. This technique will be employed in the measurement program, and the results will be compared to those obtained using filtered air.

The apparatus will be calibrated by replacing the aerosol in the White cell with a gas whose absorption coefficient is well known. At present, CH_4 is the prime candidate for this application. This method will provide a calibration of the apparatus at the same attenuation levels as expected for the aerosols.

2.2.2 Description of the Optical Train and the White Cell

The DF laser shown in Figure 2.1 is a Model 203 Lumonics TEA laser. Operating in an unstable resonator configuration with a diffraction grating in the cavity, the laser can be tuned to give an output consisting of a single line with a superradiant background. In the far field, the single line constitutes the central core of the beam and is diffraction-limited, with a divergence of $\theta_d = 0.15$ mrad. The superradiant background forms satellite rings around the central spot and has a divergence of approximately 1.0 mrad. With spatial filtering, this background can be removed, leaving a single-mode, diffraction-limited beam as the usable output from the laser. The beam diameter at the exit of the laser is typically 3.5 cm.

The energy output of the laser is typically 50 millijoules per pulse, and varies by ±5% from shot to shot. The temporal width of the pulse is approximately 1 μsec, with an initial spike 0.2-μsec wide, containing approximately 40% of the total pulse energy. A schematic of the laser pulse shape is shown in Figure 2.2.

The spatial filter shown in Figure 2.1 consists of two aluminum coated, 18^o off-axis paraboloids purchased from the Perkin Elmer Corporation. Indicated as M_1 and M_2 in the figure, these mirrors have a 312 mm (12.3 in.) focal length, and a 68 x 70 mm clear aperture. The blur circle is quoted to be 0.002 in. (0.05 mm).

The aperture in the filter is a pinhole supplied by Optimation, Inc. It consists of an aperture 100 to 500 μm in diameter drilled in a 0.375 in. diameter stainless steel substrate, 0.001 in. thick. The spatial filter suggested by Lumonics Researeh is a 1.5 mrad system. For the mirrors described above, this corresponds to a 500 μm aperture.

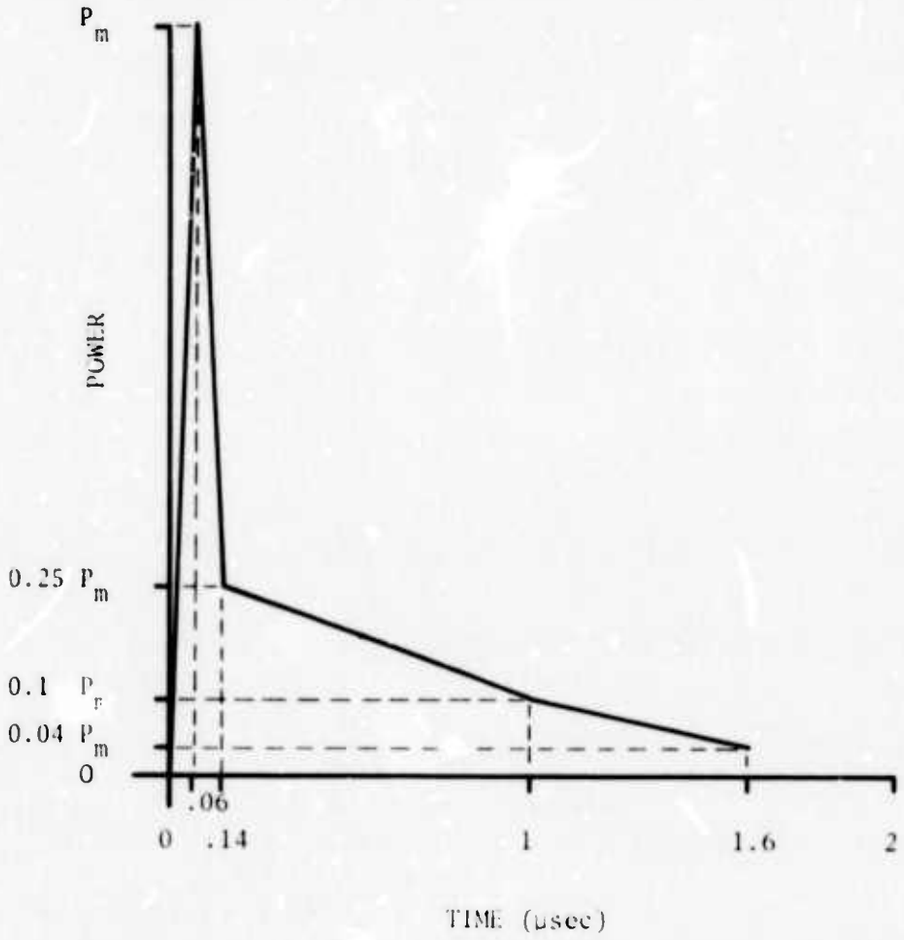

AL084

Figure 2.2 - Schematic of DF-TEA Laser Pulse Shape

To avoid laser breakdown in the vicinity of the focal volume of the spatial filter, the pinhole will be placed in a 2.5 in. diameter cylindrical vacuum chamber 6 in. in length. The chamber will be fitted with sapphire windows and will be capable of holding a vacuum of 0.1 to 1.0 torr.

The laser beam emerging from the spatial filter is diffraction limited and approximately 3.5 cm in diameter. The beam is directed by three flat mirrors, M_3, M_4, and M_5 in Figure 2.1, onto a 7.6 cm diameter, 5 meter focal length spherical mirror M_6. This mirror effectively matches the f-number of the beam to that of the White cell (f/150). With the aid of two additional flats, M_7 and M_8, the spherical mirror focuses the laser beam on the 1.5 mm entrance aperture of the cell.

Mirrors M_3 through M_8 have been supplied by PTR Optics, Inc., and they consist of a silver-coated pyrex substrate with a thorium fluoride overcoat. The mirrors are quoted to be flat to $\lambda/10$ in the visible.

The aerosol extinction coefficient will be determined by measuring the attenuation of the laser intensity as the beam traverses 80 passes in the White cell. The cell is an 8 in. diameter 6 meter long aluminum tube with three aluminum coated spherical mirrors mounted internally. The cell is being designed and fabricated by Dr. John U. White of the White Development Corporation, Stamford, CT. Provision has been made for dry nitrogen gas to flow over the mirrors to prevent these mirrors from coming in contact with the working medium in the cell. Thus, the quality of the mirrors will not degrade with time due to dust collecting on the optical surfaces. The "gas windows", however, limit the effective optical path in the cell to 5 meters per pass.

The number of passes in the cell is adjustable in units of four. Consequently, the total optical path length in the cell will be adjustable to 20, 40, 60, 80, 100, ..., 400 meters. The system is being designed to yield an output image at 3.8 μm which is diffraction limited after 20 passes. The transmission through the cell will exceed 50% after 20 passes.

The entrance and exit windows of the cell are CaF_2 windows, and because of the design of the system, the windows are insulated from the aerosol by the dry N_2 gas flow. Also included in the cell is a CaF_2 45^o beam splitter which will split off approximately 10% of the incoming beam and direct that portion onto the detector D_3.

No focusing optics are required for either detector D_3 or D_4 since each is within 10 cm of the focused laser beam. The beam diameter at the focal plane is 1.5 mm for the f/150 system, while the detector size is 2 mm diameter.

The alignment of the White cell, as well as the entire optical system, will be performed with the assistance of the Spectra Physics Model 155 He-Ne laser shown in Figure 2.1. The output from this 0.5 mw CW laser will be passed through a beam expander to match the beam diameter and divergence to those of the DF laser. The 0.6328 μm beam will then be made collinear with the DF beam with the use of a turning flat, M_0, and a CaF_2 beamsplitter, BS_1. Since the optical system contains no refractive elements (excluding the spectrometer), it is ideally suited for alignment with the visible beam.

The spectrometer shown in Figure 2.1 will be used to calibrate the diffraction grating located inside the laser cavity. The grating tunes the cavity to the desired laser line. In addition, the spectrometer will permit an evaluation of the effectiveness of the spatial filter in removing the superradiant background from the laser output.

Tentative plans call for the use of a Jarrel Ash Mark V 0.5 meter Ebert scanning spectrometer.

2.2.3 Detection System

The detectors used in the extinction measurement, D_3 and D_4 in Figure 2.1, are Model kT-1120S pyroelectric detectors manufactured by Laser Precision, Inc. Each unit is supplied with a Model kTM-333 preamplifier and a Model kTM-900 fixed load resistor. The active element size is 2.0 mm diameter. The electronic characteristics for each detector are listed in Table 2.1. Although each unit is also supplied with a variable load up to $10^{10}\Omega$, only the fixed load corresponding to a 10 MHz bandwidth is listed. The recommended maximum output from these detectors is approximately 1.0 volt. At higher output levels, the detectors approach their saturation levels.

TABLE 2.1 CHARACTERISTICS OF LASER PRECISION, INC. kT-1120S PYROELECTRIC DETECTORS WITH kTh-333 PREAMPLIFIERS AND kTM-900 FIXED LOAD MODULES

Detector	Current Responsivity (μ amp/watt)	Capacitance (pf)	Load Resistor (Ω)	Voltage Responsivity (volt/watt)	RC Time Constant (nsec)
D_3	1.51	53.1	270	4.08×10^{-4}	14.3
D_4	1.23	74	200	2.46×10^{-4}	14.8

The electronics to be used with these detectors are outlined in Figure 2.3. The output from each kT-1120S/kTH-333 detector-amplifier unit is fed into an Analog Devices, Inc. Model 50K wideband amplifier. This acts as a buffer amplifier to null the difference measurement when no absorber is in the White cell. The output from each buffer is fed into a Tektronix 1A5 differential amplifier which performs the differencing (V_o-V). Here V_o is the reference voltage from D_3, and V is the signal voltage from D_4. The signal (V_o-V) is then displayed on a Tektronix 556 dual-beam oscilloscope. The reference signal V_o will also be displayed on the oscilloscope so that for every laser pulse, the traces can be read and the ratio $(V_o-V)/V_o$ can be determined.

The oscillograms obtained with this system will provide enough data so that $(V_o-V)/V_o$ can be determined for any point during the laser pulse. The procedure will be tedious, however, since two traces must be read point-by-point and the desired radio must be calculated by hand. Therefore, when it has been amply demonstrated that the detection system is operating properly, the electronics will be modified so that $(V_o-V)/V_o$ will be determined electronically. To do this, the output (V_o-V) from the 1A5 differential amplifier and V_o from the buffer amplifier will be fed into an Analog Devices, Inc. Model 429 wideband divider. This divider is fast enough to take the ratio $(V_o-V)/V_o$ as a function of time throughout the laser pulse. However, at the 10 MHz bandwidth necessary to observe the spike at the leading edge of the laser pulse, the nonlinearity of the divider is approximately 40% for the anticipated signal levels. At 1 MHz bandwidth, this nonlinearity decreases to 5%. Therefore, the divider will provide an accurate ratio $(V_o-V)/V_o$ for the long flat tail of the laser pulse which lasts for 1 to 2 μsec.

Besides D_3 and D_4, two auxiliary detectors will be employed in the system during the extinction measurement. Detector D_2, shown in Figure 2.1, is a Laser Precision, Inc. kT-1120S detector with a kTH-333 preamplifier and a kTM-900 fixed load module. This detector will be used in conjunction with the spectrometer to monitor the spectral content of the laser pulse.

In addition, detector D_1 is a Gen-Tec, Inc. Model ED-200 joulemeter that will be used to measure the energy in each laser pulse. Detectors D_1 and D_2 will provide sufficient diagnostics to monitor the performance of the laser during the measurements.

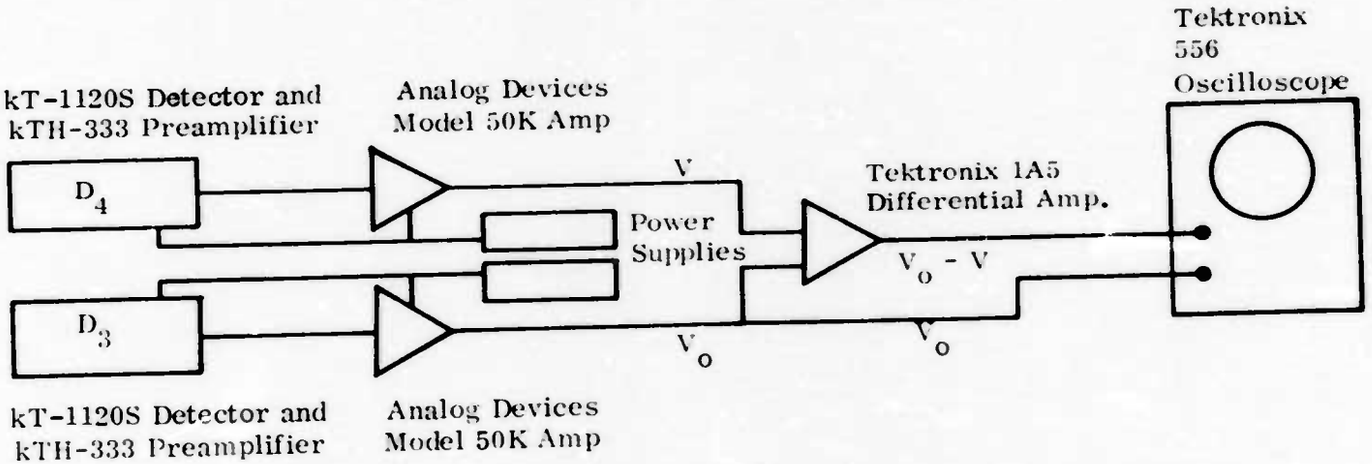

a. EXTINCTION MEASUREMENT AT SHORT TIMES (10 MHz Bandwidth)

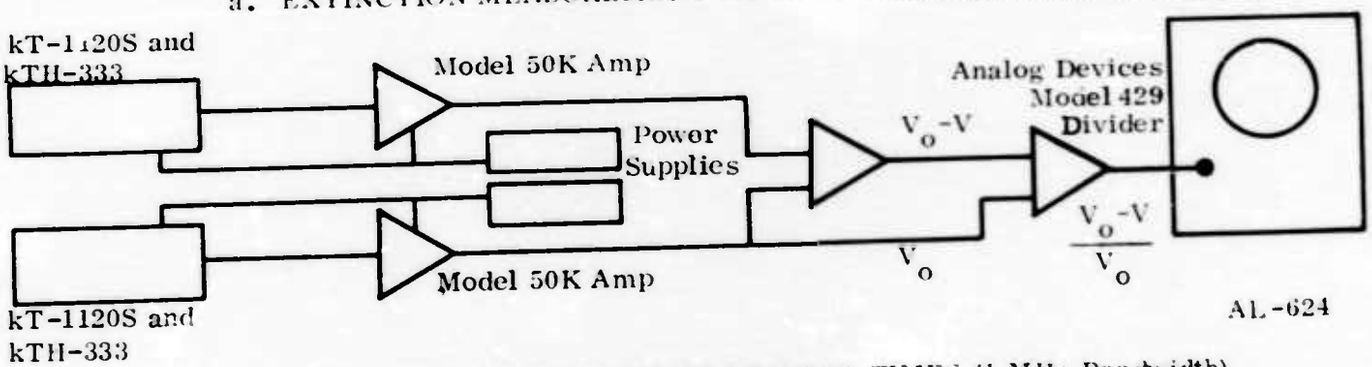

b. EXTINCTION MEASUREMENT AT LONG TIMES (1 MHz Bandwidth)

Figure 2.3 - Schematic of Electronics for Extinction Measurement

2.2.4 Aerosol Handling System

An external view of the White cell is shown schematically in Figure 2.4. The entrance and exit ports for the aerosol and the dry N_2 are surrounded by plenum chambers to ensure uniform radial flow. The aerosol is introduced into the cell through the plenum chamber at the center of the cell. Inside the plenum chamber, the aerosol is introduced into the White cell through eight sample inlet holes equally spaced around the circumference of the cell. The inlet ports for the dry N_2 that is used for the "gas window" are enclosed in the plenum chambers which are located at each end of the White cell. The exhaust ports for both the aerosol and the dry N_2 are inside the remaining two plenum chambers.

The aerosol will be drawn from the roof of the building down through the system by means of a blower located downstream of both the White cell and the scattering cell. A schematic of the aerosol and gas handling systems is shown in Figure 2.5. The flow of aerosol through each cell is monitored and balanced using standard flow meters. This is especially important in the operation of the White cell where the aerodynamic window flow must be matched to the aerosol flow. Maximum flow rate is 94 liter/min corresponding to an aerosol residence time of 0.9 min in the White cell.

The meteorological conditions at the time the aerosol is sampled will be monitored by a Heathkit Model ID-1290 weather station. This instrument will provide the wind speed and direction at the point where the aerosol is drawn into the building, approximately 10 ft above the roof. The barometeric pressure and both the outdoor and indoor temperatures will also be recorded.

The water content in the atmosphere will be measured with a Yellow Springs Instrument Company Model 91HC dew point hydrometer. The lithium chloride sensors will be placed on the roof where the aerosol is sampled and at the entrance port of the White cell and the scattering cell in the laboratory. Finally, the temperature of the aerosol-laden air will be monitored with Yellow Springs Instrument Company calibrated thermistors located on the roof and in each cell. These sensor locations are indicated by H, T in Figure 2.5.

2.2.5 Calibration Procedure

The experimental apparatus is sensitive enough to measure the attenuation of the DF laser radiation by atmospheric aerosols. The radiation on the primary and reference detectors, D_4 and D_3, respectively, is so intense that the signal-to-noise

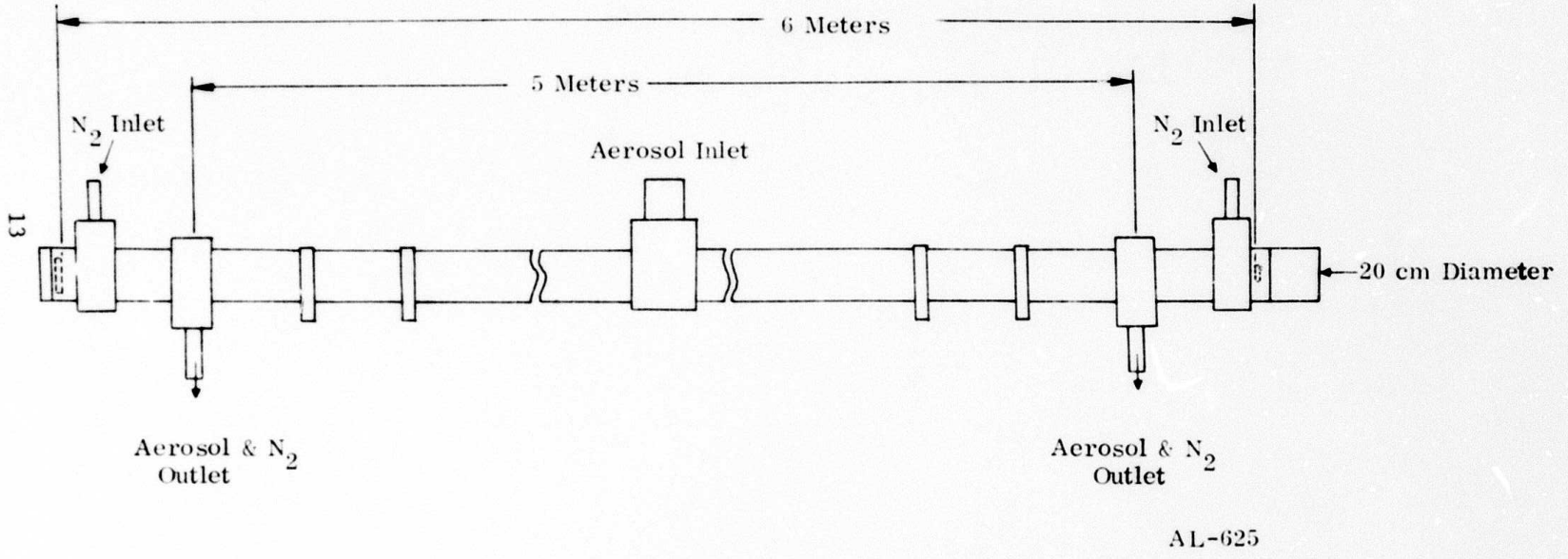

Figure 2.4 - External View of 400 Meter White Cell

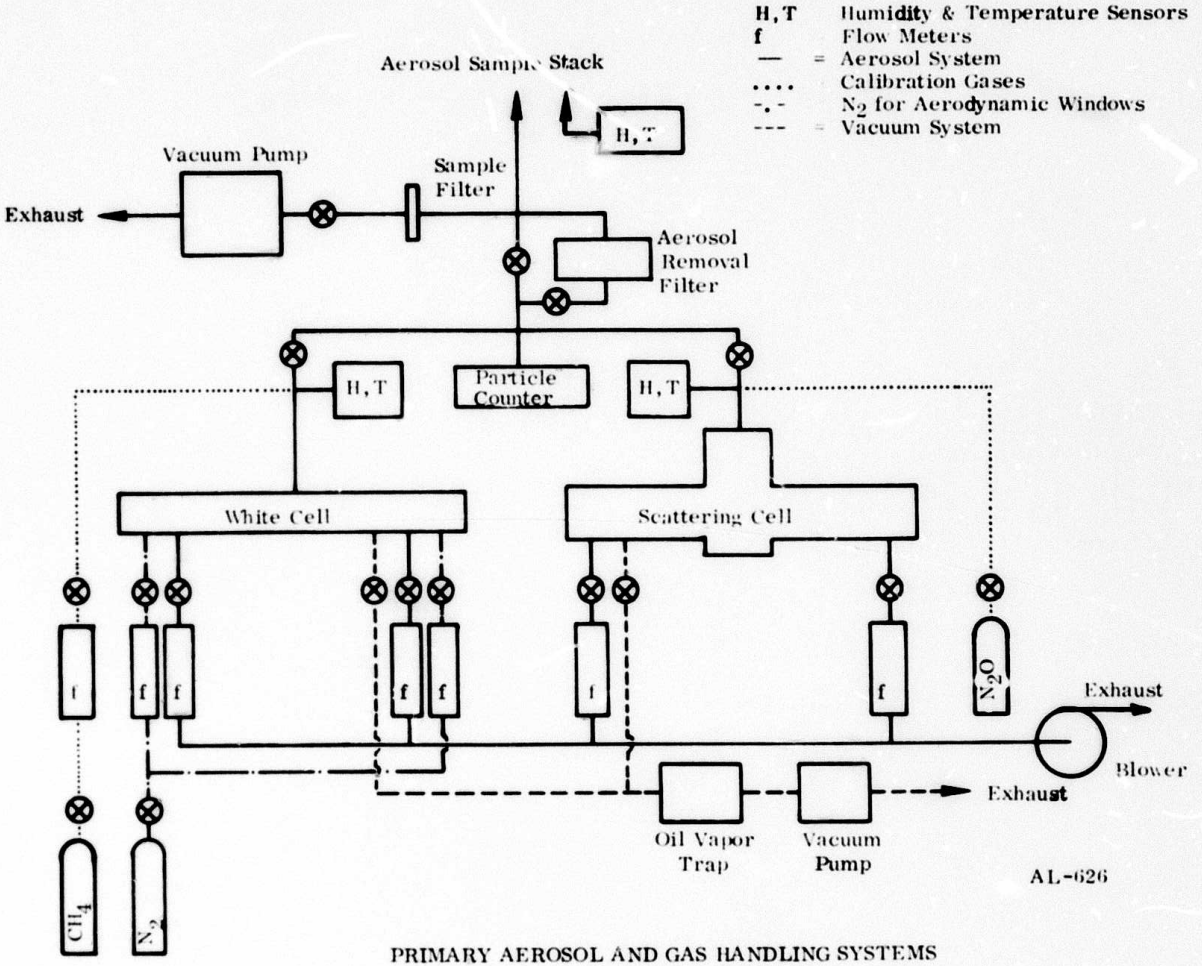

Figure 2.5 - Primary Aerosol and Gas Handling Systems

ratio in each detector is greater than 10^4 for each laser pulse. Consequently, a differential amplifier can be employed to its fullest advantage so that the attenuation can be determined to one part in 10^4. However, to establish the validity of the data and to determine the measurement accuracy, a thorough calibration procedure must be followed. Outlined in the present section are the methods by which detector linearity, alignment of the optical train, and laser stability will be verified. In addition, a dynamic calibration will be described which would allow a direct comparison of the measured aerosol extinction coefficient with the absorption coefficient of a gas as measured in other laboratories.

The Lumonics laser operated with DF can produce 50 millijoule per pulse per line with a peak power of 1×10^5 watts. With suitable attenuation, the laser can be used to calibrate the response of both detectors over a dynamic range extending from saturation down to the noise level of the detectors. Such a measurement will be performed with the White cell removed from the system, and with the laser beam focused directly into the detectors. This will provide a direct determination of the linearity of both detectors, with the critical requirement being that the quantity $(V_o - V)/V_o$ must be constant over the entire pulse. In fact, linearity itself is not critical if the response of each detector is known as a function of incident intensity. Any nonlinearity, if measured, can be corrected in the attenuation data.

Once the response of each detector has been established over the operating range of interest, a similar test can be performed with the empty White cell in the optical train, i.e., with the apparatus shown in Figure 2.1. Comparison of these results with those obtained without the White cell will indicate the degree to which the optical system is aligned. Since the aberrations produced by a properly aligned cell are astigmatic, and these can be shown to be negligible,[1,2] unsatisfactory results of this test indicate a gross misalignment of the cell and/or the focusing optics before and after the cell.

A successful calibration performed in this manner ensures proper alignment of the optical system. In addition, consistent results on successive pulses is a demonstration of the shot-to-shot spatial stability of the laser output.

In addition to the alignment check and the determination of the detector response as a function of incident intensity, a dynamic calibration will be performed which will relate the aerosol extinction coefficient to a known absorption coefficient of a gas at the same wavelength.

In essence, this calibration is an attenuation measurement with the White cell filled with a gas whose absorption coefficient is known at the DF laser line. A first choice for this application is CH_4, although other gases such as HDO could also be employed. As with the aerosol measurements, the first step in the calibration will be to take data when the White cell is empty. This determines a zero reference, and ensures one of the fact that the measured voltages can be related to the extinction coefficient by Eq. (2.2). Otherwise, that equation would have to be replaced by

$$\frac{V_o - V}{V_o} = 1 - \frac{\beta}{\gamma} \exp(-k_{ext} L) \simeq 1 - \frac{\beta}{\gamma} \left[1 - k_{ext} L + (k_{ext} L)^2/2\right] \quad .$$

Here, β and γ are constants which account for the presence of beamsplitters in the optical train, and for the (constant) difference between the responsivity of the two detectors. Nulling the signal with an empty cell simply guarantees that $\beta/\gamma \equiv 1$.

When the calibration has been completed, the White cell will be filled to one-atmosphere pressure with a $CH_4 - N_2$ gas mixture. The absorption coefficient for CH_4 in N_2 at 298^oK is shown in Figure 2.6 as a function of CH_4 partial pressure. The values shown apply to the center of the $P_2(8)$ line of DF, and are values measured recently by Spencer.[3]

The corresponding attenuation by CH_4 at the center of the $P_2(8)$ line is also shown in Figure 2.6 for a 400m path length. For CH_4 partial pressures in the range of 10^{-5} to 10^{-3} atm, the $CH_4 - N_2$ mixture provides the same attenuation expected by aerosols. Therefore, after the detector linearity and the alignment of the optical train have been checked, the dynamic calibration will be performed to verify that, in fact, the entire system is operating properly.

This calibration, performed at several laser lines, will achieve the additional goal of measuring the exact optical path in the White cell. This path length depends critically upon the location of the interfrace between the absorbing medium and the dry N_2 from the gas windows. Therefore, the path length must be determined under the flow conditions to be employed in the aerosol measurements.

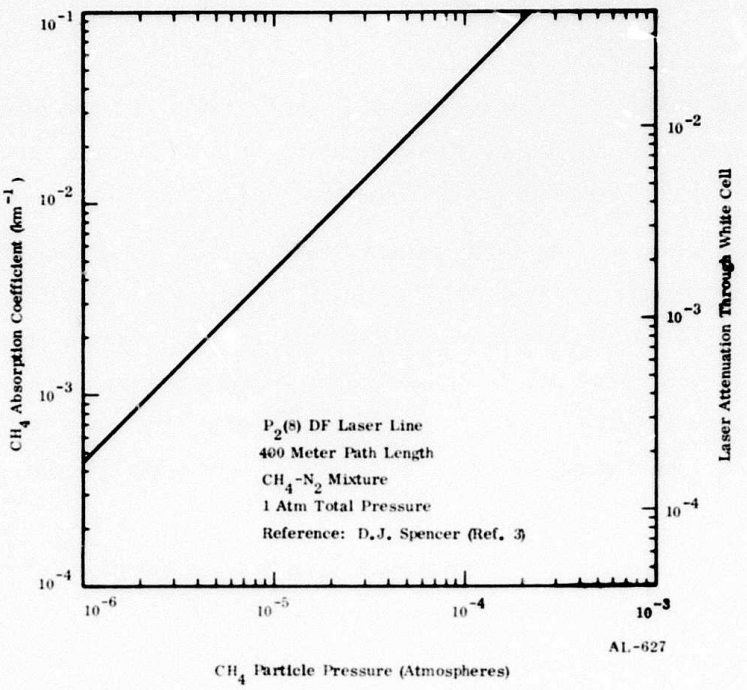

Figure 2.6 - Calibration for Extinction Measurements. Attenuation by CH_4

2.2.6 Measurement Sensitivity

The experimental apparatus is capable of providing enough data in one laser pulse to determine the aerosol extinction coefficient. However, the accuracy of the measurement is determined by the relevant signal-to-noise ratios in the system.

As mentioned earlier and as shown in Table 2.1, detectors D_3 and D_4 in Figure 2.1 are Model kT-1120S pyroelectric detectors with voltage responsivities of $R_v = 2.4 \times 10^{-4}$ and 4.1×10^{-4} volt/watt, and a maximum unsaturated output of 1.0 volt. This corresponds to inputs of 4.2×10^{3} and 2.4×10^{3} watts, respectively. The maximum incident laser energy is 6.4 millijoule per pulse. The detector self-noise is Johnson noise, which for a 200Ω load and 10-MHz bandwidth is 5×10^{-6} volts, or approximately 0.015 watt.

The maximum power of the DF laser pulse as shown in Figure 2.2 is $P_M = 3.5 \times 10^{6} E_o$ watts, where E_o is the total pulse energy, and the power at the base of the initial spike is $P \simeq 0.25 P_M$. Consequently, for $E_o = 0.006$ joule, $P_M = 2.1 \times 10^{4}$ watts and $P \simeq 5.3 \times 10^{3}$ watts. For 1.0 millijoule incident energy, $P_M = 3.5 \times 10^{3}$ and $P = 8.75 \times 10^{2}$ watts.

The signal-to-noise ratios calculated in this section will use the power at the base of the laser spike, so that it should be borne in mind that the results must be increased by a factor of four to apply at the peak of the pulse.

Using the Johnson noise of the detectors and $P = 8.75 \times 10^{2}$ watts, one finds that the signal-to-noise ratio at detectors D_3 and D_4 is approximately 5.8×10^{4}. However, the signal-to-noise ratio for the differential measurement is the ratio of $(V_o - V)$ to the largest noise source in the system. Since the measurement will be performed with the Tektronix 1A5 differential amplifier, the noise source is the amplifier itself, whose noise level is $V_N = 5 \times 10^{-5}$ volt rms. Therefore,

$$\frac{S}{N} = \frac{V_o - V}{V_N} = \frac{V_o \left(1 - e^{k_{ext} L}\right)}{V_N} \simeq \frac{V_o k_{ext} L}{V_N} \quad . \tag{2.3}$$

The reference signal V_o is simply the product of the voltage responsivity, R_v, and the incident laser power, P. Under these conditions, the signal-to-noise ratio is approximately

$$\frac{S}{N} = \frac{R_v P k_{ext} L}{V_N} = \frac{(3 \times 10^{-4})(8.75 \times 10^{2}) k_{ext} (0.4)}{5 \times 10^{-5}} \quad ,$$

that is,

$$\frac{S}{N} = 2100 \, k_{ext} \quad , \tag{2.4}$$

where the extinction coefficient is in units of km^{-1}. This is the achievable signal-to-noise ratio per pulse. For an extinction coefficient of $k_{ext} = 3 \times 10^{-3} \ km^{-1}$, a conservative lower bound on the expected value, the signal-to-noise ratio will be $S/N \simeq 6$.

The signal-to-noise ratio for the measurement of V_o from the reference pulse ahead of the White cell is the same as the above, except that the factor $k_{ext} L$ is replaced by 10^{-1}, the fraction of incident power split off onto D_3 by the beamsplitter at the entrance of the White cell. Also, the dominant noise is now the Johnson noise of the detector, since the differential amplifier is not used to measure V_o. Therefore, $V_N = 5 \times 10^{-6}$ volts, and the corresponding signal-to-noise ratio is $S/N = 5.3 \times 10^{3}$.

The accuracy with which one can determine the extinction coefficient from this measurement depends upon the signal-to-noise ratio and the accuracy to which one can read the oscilloscope traces which display $(V_o - V)$ and V_o. The relevant signal-to-noise ratio is given by Eq. (2.4). The error incurred by reading an oscilloscope trace is typically ±5%. Thus, the error in k_{ext} is the rms value of these contributions,

$$\epsilon_{ext} = \left[(S/N)^{-2} + (0.05)^2\right]^{1/2}$$
$$= \left[2.3 \times 10^{-7}/k_{ext}^{\ 2} + 2.5 \times 10^{-3}\right]^{1/2} \qquad (2.5)$$

This assumes that the ratio $(V_o - V)/V_o$ is obtained electronically. If, instead, $(V_o - V)$ and V_o are read individually, then a factor of 2 should appear before the first term in the brackets in Eq. (2.5)

A plot of Eq. (2.5) is shown in Figure 2.7. As shown in the figure, the extinction coefficient can be determined to within 50% when $k_{ext} \simeq 10^{-3}$ km^{-1}, the lowest value of interest. For $k_{ext} \simeq 10^{-2}$ km^{-1}, the error is ±7%.

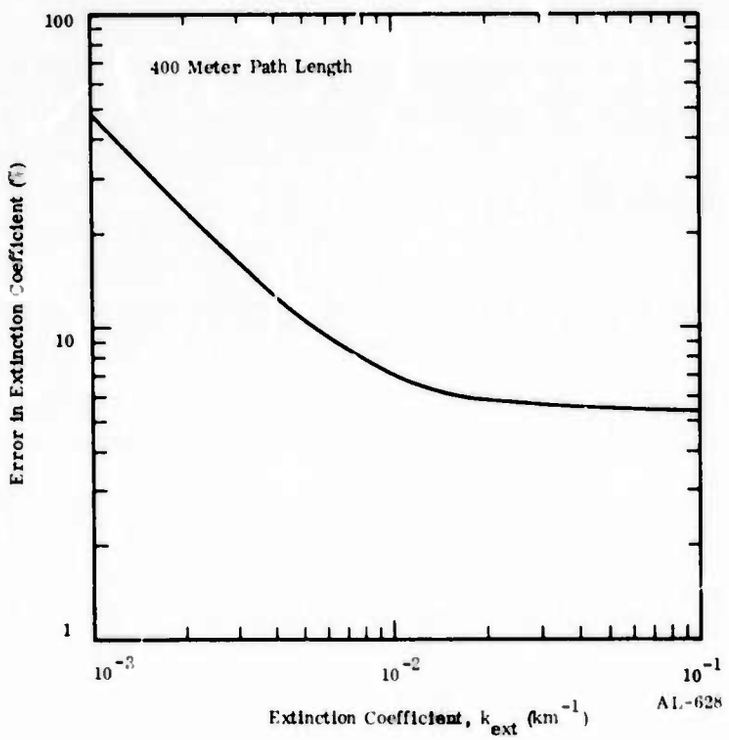

Figure 2.7 - Accuracy of Measured Extinction Coefficients

2.3 Scattering Measurement

2.3.1 Theory of the Measurement

The scattering coefficient of the atmospheric aerosol will be determined from a measurement of the intensity of radiation scattered out of a parallel laser beam as the beam traverses a 4.5 meter cell containing the aerosol. An infrared detector will be placed several centimeters from the axis of the laser beam and will monitor the scattered radiation with a field-of-view of approximately 170^{o}. A schematic of the region around the detector is shown in Figure 2.8.

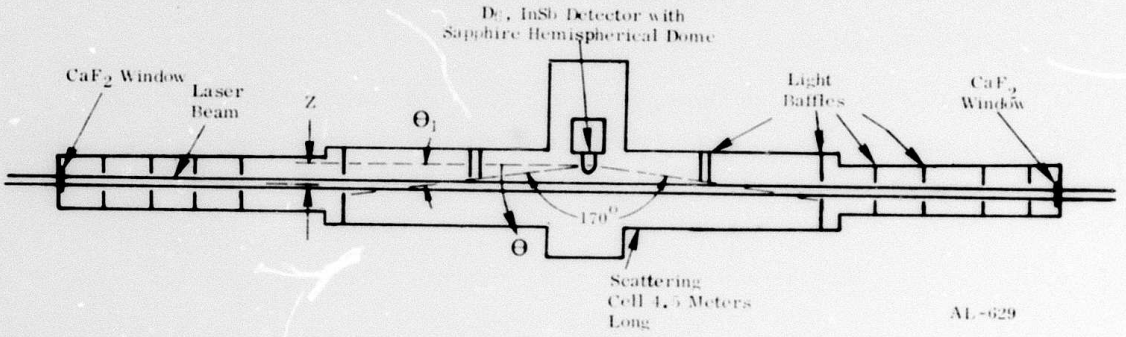

Figure 2.8 Schematic of Aerosol Scattering Cell

The experimental arrangement for the scattering measurement is straightforward, and it permits one to obtain a direct measurement of the scattering coefficient in a single laser pulse if stray background radiation has been properly suppressed. This can be shown by calculating the signal for the arrangement shown in Figure 2.8. Let the beam intensity be I_o watts/cm^2 and the beam area be A_B. The detector has an area A_d, and is placed at a distance Z from the beam. The signal that one observes is given by the relation

$$P_{scat} = \int_o^{\infty} \int_V I_o \, n(r) \, \sigma(r,\theta) \, \Omega_d \, dV \, dr \quad . \qquad (2.6)$$

The integration is over the volume V occupied by the laser beam, and over the particle size distribution, n(r). In Eq. (2.9), r is the particle radius; σ is the scattering cross section, a function of r and θ ; and Ω_d is the solid angle of the detector, as seen from the volume element dV. If we let x be the coordinate along the beam, then $dV = A_B\, dx$. The total beam power can be written as $P_o = I_o A_B$, and the detector solid angle is

$$\Omega_d = \frac{A_d \sin\theta}{x^2 + Z^2} \quad . \tag{2.7}$$

The factor $\sin\theta$ transforms the detector area to the projected area seen from the volume element dV. Inserting these expressions into Eq. (2.6) yields

$$P_{scat} = P_o \int_o^\infty \int_{-\infty}^\infty n(r)\, \frac{\sigma(\theta, r)\, A_d \sin\theta}{x^2 + Z^2}\, dx\, dr \quad . \tag{2.8}$$

By using the relation $x = Z \cot\theta$ to transform from the x- to the θ-coordinate, the signal becomes

$$P_{scat} = \frac{P_o A_d}{Z} \int_o^\infty \int_o^\pi n(r)\, \sigma(\theta, r) \sin\theta\, d\theta\, dr \quad . \tag{2.9}$$

Since the scattering cross section is related to the scattering coefficient, k_{scat}, by

$$k_{scat} = 2\pi \int_o^\infty dr \int_o^\pi \sin\theta\, n(r)\, \sigma(r, \theta)\, d\theta \quad , \tag{2.10}$$

one obtains a relation between the signal and the scattering coefficient,

$$P_{scat} = \frac{P_o A_d}{2\pi Z}\, k_{scat} \quad \text{watts} \quad . \tag{2.11}$$

In the ideal case described by Eqs. (2.9) and (2.11), the beam would be observed from $x = -\infty$ to $x = +\infty$, or for the range of angles from $\theta = 0^o$ to $\theta = 180^o$. However, this cannot be achieved in the laboratory because the radiation scattered from the side walls and end plates would be seen by the detection system. Instead, baffles limit the range of viewing angles from θ_1 to $(180^o - \theta_1)$, precluding observations of forward and backward scattering. This corresponds to offsetting the detector by the distance Z = 5.3 cm and 11 cm from the beam for $\theta_1 = 10^o$ and 20^o, respectively. This distance should be short in order to minimize θ_1.

Most of the aerosol particles are contained in the size range less than 1 μm. The scattering cross section $\sigma(\theta, r)$, on the assumption of spherical aerosol particles, is expected to be only a weak function of scattering angle θ, so that $\sigma(\theta, r) \sim \cos^2 \theta$ is a good approximation. Since the scattering cross section does not peak strongly at 0^o and 180^o, the errors involved in the truncation are not serious, approximately 10% and 17% for $\theta_1 = 10^o$ and 20^o, respectively. Thus, a good measurement can be obtained even without observing the forward and backward directions.

The scattering coefficient is obtained by solving Eq. (2.11),

$$k_{scat} = \frac{2 \pi Z P_{scat}}{P_o A_d} \quad . \tag{2.12}$$

2.3.2 Description of the Apparatus

The experimental apparatus for measuring the atmospheric aerosol-scattering coefficient is shown in Figure 2.1. A beamsplitter directs only a small portion of the laser radiation to the White cell. The major portion of the beam (~90%) passes through the scattering chamber. The chamber is a tube 30 cm in diameter and 4.5m long, with the laser beam propagating along its axis. Annular disc diaphragms are placed in the tube to suppress radiation scattered from the walls (see Figure 2.8). A Santa Barbara Research indium antimonide infrared detector is located equidistant from the ends of the chamber to maximize the distance to the end windows. The detector, 2.0 mm in diameter, is placed several centimeters away from the beam, and observes radiation scattered from the medium. The detector is fitted with a sapphire hemispherical dome to minimize reflection losses at the detector window for rays striking the detector at shallow angles of incidence.

The photovoltaic detector is liquid nitrogen cooled and has a D* of 2.4×10^{10} cm-Hz$^{1/2}$/watt at 3.8 μm. This corresponds to a NEP of 2.3×10^{-8} watts for a 10 MHz bandwidth.

Baffles placed near the detector eliminate the stray light scattered from the walls of the chamber and from the windows in the end walls. The disc baffles closest to the detector are 1m away on each side. These discs perform the major baffling of the light, while inner secondary baffles on the detector side remove the light scattered from the closest discs.

The referenee intensity for the seattering measurement will be determined by deteetor D_5 shown in Figure 2.1. Thi.. is a Laser Precision, Inc. Model kT-1520S pyroeleetrie deteetor with a 2 mm diameter element. The deteetor's eapaeitanee is 25 pf, and eurrent responsivity of 1.66 μamp/watt. For a 50Ω load, this corresponds to an RC time eonstant of 12.5 nsee and a voltage responsivity of 8.3×10^{-5} volts watt. For a 10 MHz bandwidth and a 50Ω load, the self-noise is 3×10^{-6} volts or 0.036 watt.

Approximately 10% of the laser intensity is directed onto D_5 by a CaF_2 beam-splitter, BS_4, loeated in front of the entranee to the seattering eell. As for the detectors used in the extinetion measurement, deteetors D_5 and D_6 will be aligned with the assistanee of the He-Ne laser.

As for the White eell, the aerosol will flow through the seattering eell during the measurement. Coming from the same manifold which supplies the White eell, the aerosol will enter the seattering eell at the eenter near deteetor D_6, and will flow out of the eell at eaeh end. Flowmeters at the exit ports will eontrol the flow rate. As mentioned in Subseetion 2.2.4, the temperature and water vapor eontent will be monitored inside the eell.

2.3.3 Calibration Proeedure

In order to perform measurements of absolute scattered intensities, one must determine the solid angle and sensitivity of the deteetor, the gain of the electronics, and the beam diameter and power density of the laser. In prineiple, these quantities ean be ealculated, determined from manufaeturers' speeifieation, or in the ease of the laser power, measured in the laboratory. Alternatively, if a souree of known intensity at 3.8 μm is available whieh has the same geometrie shape as the seattering volume, then the measurement of the signal strength from this souree will yield an overall responsivity of the detection system. This responsivity will eontain all the unknown faetors in the system, and will eliminate the need for the error-prone analysis indieated above.

An example of such a souree is the 3.8 μm fluoreseenee from a known molecular system following absorption of DF laser radiation. In this ease, the same DF laser is used so that the source geometry is identical to that for the scattering measurement. Moreover, if the fluoreseenee measurement is performed in the first few mieroseconds following the laser pulse, then the ealibration is earried out over a time scale eomparable to that for the scattering measurement.

Initially, it was proposed that the molecular system consist of a properly chosen mixture of DF and CO_2. The DF would absorb the laser energy and transfer the bulk of it to CO_2 by collisions. The CO_2 would then radiate in its intense 4.3 μm band. The intensity is a calculable quantity expressed in terms of the DF absorption coefficient and the CO_2 radiative lifetime.

Unfortunately, such a scheme requires additional equipment in the form of a mixing chamber for the gases. Moreover, since the available scattering chamber has a relatively large volume (~250 liters), and this kinetic scheme requires DF partial pressures of $\sim 10^{-1}$ atm, a substantial amount of toxic DF gas would be required.

To avoid these difficulties, the DF-CO_2 system has been replaced by pure N_2O. The absorption coefficient for N_2O has been measured previously[3] at several DF laser lines. The data indicate that at the $P_2(11)$ ($\lambda = 3.9155\ \mu$m) and the $P_3(8)$ ($\lambda = 3.9272\ \mu$m) laser lines, absorption by N_2O is strong enough to permit the calibration to be performed at gas pressures in the range of 50 to 200 torr. At these levels, collisional quenching of $N_2O(20^00)$, the upper level in the absorption process, is insignificant during the laser pulse. Consequently, at the end of the pulse, the population of the radiating state is given by

$$\begin{aligned}\left[N_2O(20^00)\right] &= \left[N_2O(00^00)\right] \sigma_r \frac{E_o}{A_B} \left(\frac{\lambda}{hc}\right) \exp(-t/\tau) \\ &= k_r \frac{E_o}{A_B} \left(\frac{\lambda}{hc}\right) \exp(-t/\tau) \quad .\end{aligned} \tag{2.13}$$

Here σ_r and $k_r = \left[N_2O(00^00)\right] \sigma_r$ are the absorption cross section and absorption coefficient, respectively, E_o is the laser pulse energy, and hc/λ is the laser photon energy. The quantity τ is the time constant for the relaxation of the $N_2O(20^00)$ both by collisions (τ_o) and radiative decay (τ_r). Thus, $\tau^{-1} = \tau_o^{-1} + \tau_r^{-1}$. The time t is measured from the end of the laser pulse.

In the measurement geometry shown in Figure 2.8, the InSb detector is oriented 90° to the laser axis and has a field-of-view of approximately 170°, i.e., $\theta_1 \simeq 5^o$. Under these conditions, the N_2O emission is given by

$$P_{N_2O} = \int_{Vol} \frac{\left[N_2O(20^00)\right]}{\tau_r} \frac{hc}{\lambda} \frac{\Omega_d}{4\pi} \, dVol \tag{2.14}$$

where the integration is performed over the gas volume irradiated by the laser beam. Expressing solid angle and the volume element in terms of x, θ, and Z, one can evaluate the integral and obtain for the N_2O emission incident on the detector

$$P_{N_2O} = \frac{\left[N_2O(20^00)\right]}{\tau_r} \frac{hc}{\lambda} \frac{A_B A_d}{2\pi Z} \quad . \tag{2.15}$$

With Eq. (2.13), the fluorescence signal strength can be expressed as

$$P_{N_2O} = \frac{k_r}{\tau_r} \frac{E_o A_d}{2\pi Z} \exp(-t/\tau) \quad \text{watts} \quad . \tag{2.16}$$

Therefore, the calibration intensity is a simple function of the measurable parameters E_o, A_d, and Z, and of the radiation parameters k_r and τ_r.

As mentioned above, k_r has been determined in other laboratories. The radiative lifetime, τ_r, can be calculated directly from previous band intensity measurements,[4] and is found to be $\tau_r = 133$ msec for the $N_2O(20^00)$-(00^00) band at 3.90 μm. The rate constant for collisional deexcitation of $N_2O(20^00)$ in pure N_2O is estimated to be $k_c \simeq 10^{-14}$ cm^3-sec^{-1}, so that the time constant for collisional quenching is

$$\tau_c \simeq \frac{4 \times 10^{-6}}{p_{N_2O}} \quad \text{sec},$$

where p_{N_2O} is the gas pressure in atmospheres. Therefore, the time constant in Eq. (2.16) is given by $\tau \simeq \tau_c$. For $50 \leq p_{N_2O} \leq 200$ torr, (i.e., $0.066 \leq p_{N_2O} \leq 0.263$ atm), τ assumes values in the range of $15 < \tau < 60 \mu$sec. Consequently, during the measurement of the N_2O fluorescence, ($0 \leq t \leq 2 \mu$sec), collisional quenching is insignificant, and the signal strength may be approximated by

$$P_{N_2O} \simeq \frac{k_r}{\tau_r} \frac{E_o A_d}{2\pi Z} \quad \text{watts.} \tag{2.17}$$

This analysis applies to the measurement conditions provided the N_2O gas pressure is chosen so that saturated absorption is avoided. This condition is satisfied if

$$2 \sigma_r \delta \Phi < 1 \tag{2.18}$$

where $\sigma_r = k_r / \left[N_2O(00^00; J)\right]$ is the absorption cross seetion, $\delta = \left[N_2O(00^00; J)\right] / \left[N_2O(00^00)\right]$ is the ratio of the population in the lower absorbing level to that in the levels strongly coupled to the absorbing level , and Φ is the total laser photon flux in photons/cm^2. In the expression for δ, J is the rotational quantum number of the absorbing level. For the scattering measurement, the laser pulse energy is 50 millijoule and the beam diameter in the scattering cell is 3.5 cm, so that $\Phi \simeq 10^{17}$ photons/cm^2. The quantity $2\sigma\delta\Phi$ then reduces to

$$2\sigma\delta\Phi = 8 \times 10^{-3} P_r$$

at 300^{o}K. Here, $P_r = k_r/p_{N_2O}$ is the speetral absorption coefficient in cm^{-1} atm^{-1}. The inequality in Eq. (2.18) requires that $P_r < 125$ cm^{-1} atm^{-1} to avoid nonlinear saturation effects. Spencer's data[3] for N_2O absorption eoefficients at the DF laser lines show that this requirement is satisfied at all the intense laser lines for all N_2O gas pressures of interest (i.e., $\leq$ 1 atm).

The ratio of the aerosol scattered intensity to the N_2O fluorescence obtained from Eqs. (2.11) and (2.17) is

$$\frac{P_{scat}}{P_{N_2O}} = \frac{P_o}{E_o} k_{scat} \left(\frac{\tau_r}{k_r}\right) \tag{2.19}$$

Setting $P_o = P_M$, where P_M is the peak laser power given in Subsection 2.2.6 as $3.5 \times 10^6 E_o$ watts, this becomes

$$\frac{P_{scat}}{P_{N_2O}} = 4.7 \times 10^5 \frac{k_{scat}}{k_r} \tag{2.20}$$

The N_2O absorption eoefficients as measured by Spencer at the $P_2(11)$ and $P_3(8)$ DF laser lines are shown in Figure 2.9. Also indicated are the points at whieh $P_{scat} \simeq P_{N_2O}$ for $k_{scat} \simeq 10^{-3}$ km^{-1} and 10^{-2} km^{-1}. This essentially defines the N_2O pressure range at which the ealibration will be run.

This proeedure can also be run at other DF laser lines for which there is substantial N_2O absorption. The $P_2(10)$ and $P_3(7)$ lines are obvious eandidates. The selection of the particular line to be used will be determined by the choice of laser lines for the scattering measurement. Approximately eight laser lines are of sufficient intensity for the scattering measurements, and at least four of these are absorbed by N_2O.

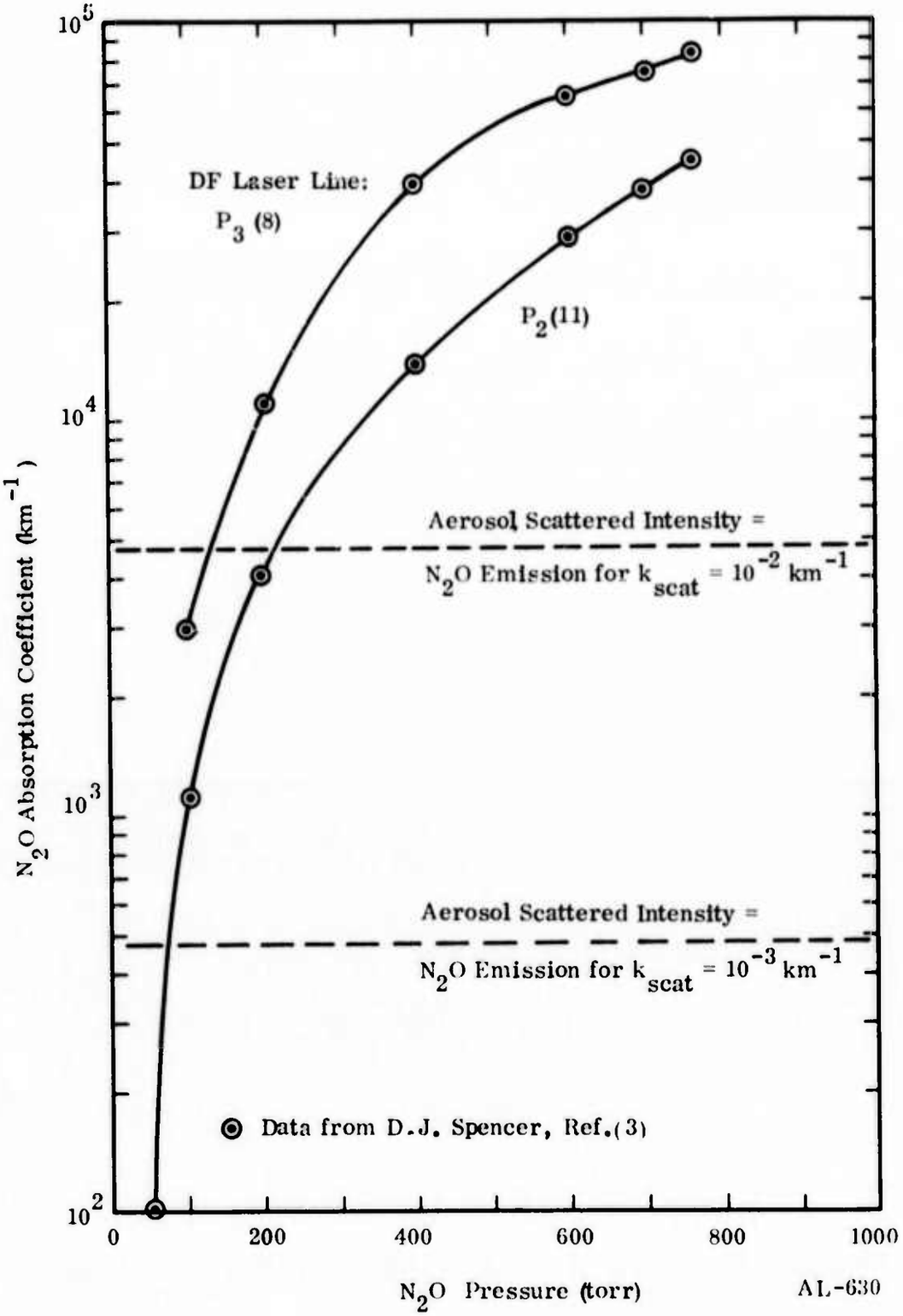

Figure 2.9 - N_2O Absorption Coefficient and Operating Levels for Scattering Calibration

2.3.4 Measurement Sensitivity

Based upon the expressions developed in Subsection 2.3.1 and the instrument parameters listed in Subsection 2.3.2, one can estimate the signal-to-noise ratio for the scattering measurement. Assuming $P_o = 1.75 \times 10^5$ watts, the peak power for 50 mj incident on the scattering cell, Eq. (2.11) yields

$$P_{scat} = 1.75 \times 10^{-3} k_{scat} \quad \text{watts},$$

if the detector is located 5 cm from the axis of the laser beam. Compared to the NEP of 2.3×10^{-8} watts for D_6, the InSb detector, this gives a signal-to-noise ratio of

$$S/N = 7.6 \times 10^4 k_{scat} \quad , \tag{2.21}$$

where k_{scat} is in km^{-1}. For $k_{scat} = 10^{-3}$ km^{-1}, a factor of ten less than the value expected for the extinction coefficient, the signal-to-noise ratio is S/N = 76. Thus with a single laser pulse, one can obtain a measurement of the scattering coefficient at the lower range of interest for the experiment.

The accuracy to which the scattering coefficient is determined by this measurement depends upon the signal-to-noise ratio given by Eq. (2.21) and the systematic errors involved in reading the signals from detectors D_5 and D_6. In addition, it is clear from Eq. (2.19) that the accuracy of the scattering coefficient also depends upon the accuracy to which (k_r/τ_r) is known for N_2O. Assuming this is ±20%, then the error in k_{scat} is the rms of all these contributions, i.e.,

$$\epsilon_{scat} = \left[(S/N)^{-2} + 2(0.05)^2 + (0.20)^2\right]^{1/2}$$

$$= \left[7.7 \times 10^{-10}/k_{scat}^{\ 2} + 4.5 \times 10^{-2}\right]^{1/2} \quad , \tag{2.22}$$

where k_{scat} is in km^{-1}. Implicit in this relation is the assumption that the outputs from detectors D_5 and D_6 can be read to ±5% from oscilloscope traces.

For $k_{scat} \geq 10^{-3}$ km^{-1}, the error is insensitive to the magnitude of k_{scat} and is approximately ±21%; i.e., the error is due primarily to the uncertainty in the calibration.

2.4 Accuracy of Absorption Coefficient Determination

The values of the measured aerosol extinction and scattering coefficients are of interest in themselves. However, the primary objective of the measurement program is to obtain values for the absorption coefficient k_{abs}. This follows directly from the data and

$$k_{abs} = k_{ext} - k_{scat} \quad .$$

The error, ϵ_{abs}, in k_{abs} determined in this way is given by

$$k_{abs} (1 \pm \epsilon_{abs}) = k_{ext} (1 \pm \epsilon_{ext}) - k_{scat} (1 \pm \epsilon_{scat})$$

so that

$$\epsilon_{abs} = \frac{k_{ext} \epsilon_{ext} + k_{scat} \epsilon_{scat}}{k_{ext} - k_{scat}} \quad .$$

Consequently, the error in k_{abs} can be expressed in terms of the ratio of the scattering to the extinction coefficient,

$$\epsilon_{abs} = \frac{\epsilon_{ext} + (k_{scat}/k_{ext}) \epsilon_{scat}}{1 - (k_{scat}/k_{ext})} \quad . \qquad (2.23)$$

As expected, the error grows rapidly as the relative contribution of the absorption to the total extinction decreases, i.e., as k_{scat}/k_{ext} approaches unity.

The expressions for ϵ_{ext} and ϵ_{scat} are given by Eqs. (2.5) and (2.22), respectively. The quantity ϵ_{ext} is a function of k_{ext}, while as stated in Subsection 2.3.4 $\epsilon_{scat} \simeq 0.21$ for all $k_{scat} \geq 10^{-3}$ km^{-1}. Therefore, the error in the absorption coefficient is determined principally by the ratio k_{scat}/k_{ext}. The dependence upon the absolute magnitude of k_{ext} is of secondary importance.

These features of the behavior of ϵ_{abs} are apparent in Figure 2.10 where ϵ_{abs} is plotted versus k_{scat}/k_{ext} for several values of k_{ext}. For the range of extinction coefficients of interest, $k_{ext} > 3 \times 10^{-3}$ km^{-1}, the error in k_{abs} is less than a factor of 2 when scattering represents less than 70% of the total extinction. For the more realistic values $k_{ext} \geq 10^{-2}$ km^{-1}, the error in k_{abs} is less than a factor of 2 when $k_{scat}/k_{ext} \leq 0.80$.

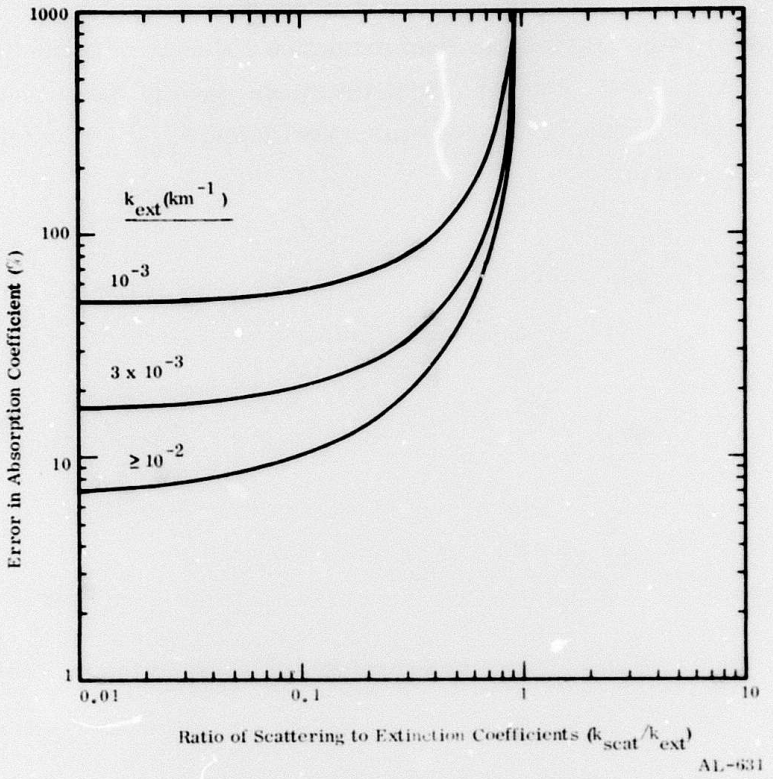

Figure 2.10 - Accuracy of Absorption Coefficient Determintation

2.5 Aerosol Characterization

Measurements will be conducted to determine the composition and characteristics of the aerosol used in the experiments described above with a two-fold purpose: first, to identify the contributions of various aerosol sources to the ambient aerosol so that the results of these studies may have more than local relevance and, second, to monitor changes in the ambient aerosol from the roof-mounted sampling inlet to the scattering and extinction cells.

Aerosol source identification will combine an elemental analysis of impacted aerosol samples with local and regional wind conditions to determine the nature of the measured aerosol. As may be seen from Figure 2.11, Aerodyne Research, Inc., (ARI) is located to the northwest of metropolitan Boston. There is no heavy industry in the area. Major components of the ambient aerosol are expected to be soil dust

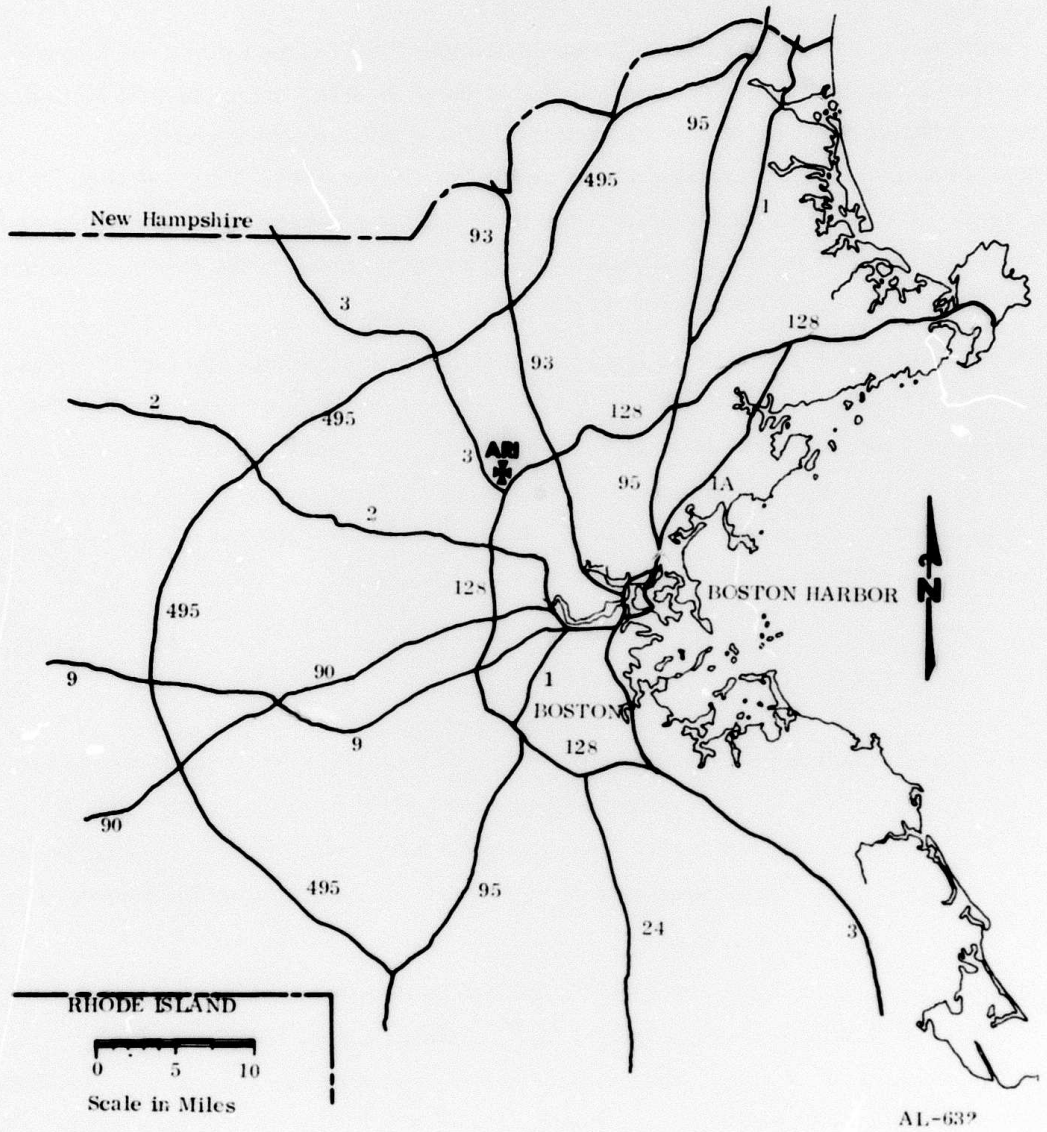

Figure 2.11 - Location of Aerodyne Research Inc.

and sea salt, the so-called continental aerosol, combined with fuel oil ash generated by the widespread use of oil in residential heating systems. The close proximity to a heavily used freeway, Route 128, will also give rise to automobile exhaust aerosols.

Analyses of chemical element composition and total aerosol mass loading will be performed by Skinner and Sherman Laboratories of Boston. Samples will be collected by impacting the aerosol on 90 mm diameter Millipore filters of 0.1 and 0.45 μm diameter pore sizes. The sampling times needed to collect above 1 mg are 8 and 0.9 hours, respectively. The larger pore filter is in common use for aerosol studies; however, it is felt that the smaller pore filter will provide a check on the contribution and effects of the more numerous smaller particles.

Source identification will be accomplished by the method of chemical element balance. In this method, the observed aerosol elemental concentration is compared with concentrations emanating from known sources. The result is a characterization of the aerosol in terms of identifiable constituents. Mathematically, if X_i is the measured concentration of element i and Z_{ij} is the percent of element i due to source j, then the problem is reduced to solving a set of i equations of the form:

$$X_i = \sum_j Z_{ij} \, m_j \qquad (2.24)$$

for the coefficients m_j which represent the mass of material from source j contained in the aerosol. Obviously, the determination of an accurate source matrix (Z_{ij}'s) is essential. Table 2.2 represents the best available literature values.[5] Contacts have been made with the EPA in hope of getting better data on automobile and fuel oil compositions.

Since the ARI sampling program is not yet underway, published elemental compositions from samples collected at MIT[6] (urban Boston) have been analyzed to illustrate the method. Table 2.3 gives the concentrations of key elements. The chemical element balance, using the source coefficients from Table 2.3, gives a set of eight equations in four unknowns. The solutions are:

Soil Dust	55%
Fuel Oil Ash	41%
Sea Salt	3%
Automobile	1%

TABLE 2.2 - SOURCE MATRIX OF KEY ELEMENTS CONCENTRATIONS

	Aerosol Source			
Element	Sea Salt	Soil Dust	Auto Exhaust	Fuel Oil
Na	30.6	2.5		5
Mg	3.7	1.4		0.06
Al		8.2		0.8
Cl	55		6.8	
V		0.006		7
Mn		2.1		0.06
Fe		3.2	0.4	6
Br	0.19		7.9	
Zn		0.006	0.14	0.02

TABLE 2.3 - METROPOLITAN BOSTON AEROSOL
(Source: Gorden, et al., 1974)

Element	Concentration (ng/m^3)
Na	1480
Al	1630
Cl	590
V	980
Mn	30
Fe	1480
Br	224
Zn	260

Total observed = 8737 ng/m^3

These results seem compatible with the windy, winter conditions prevailing during the collection.

Atmospheric aerosols are highly hygroscopic with resultant rapid size increase at relative humidities greater than 70-80% . Humidity and temperature measurements will be made at the sampling stack entrance and in each experimental cell.

A portable Royco aerosol particle counter is being obtained on loan from AFWL. It will be used to provide relative particle concentrations during the course of these experiments as well as to check for possible aerosol concentration changes between the sampling stack entrance and the experimental cells.

2.6 Program Status and Future Work

This past reporting period has been one of design, specification, fabrication, and assembly of the laboratory apparatus necessary for the experimental program. The details of the system and the specifications of most of the components have been listed in Subsections 2.1 through 2.5 of this report. Where possible, the current status has been indicated.

The system, as it has been outlined, can be divided into six subsystems: the scattering cell, White cell, optical train, detection system, laser system, and aerosol handling system. Briefly, the scattering cell has been designed and fabricated. Its associated vacuum system has been assembled, and the cell is presently being connected to the aerosol handling system. With the exception of a stray-light baffling system, the scattering subsystem is virtually complete. The White cell has been designed and is being fabricated by Dr. John U. White of White Development Corporation. The unit is scheduled for completion by mid-December 1974, and for installation at ARI within the following month. This includes the cell, its associated optical components, and the plumbing for both the aerosol and the gas windows.

The design of the optical train required to direct the laser beam into the White cell and scattering cell is complete. All necessary optical components are on hand, and the assembly has begun. The spatial filter, the most critical component of this subsystem, has been designed. The vacuum chamber that will enclose the spatial filter and will eliminate air breakdown is currently being fabricated.

The detection system for both the scattering and extinction measurements has been designed, and the necessary electronic components have been purchased. Check-out and preliminary calibration of the several detectors are scheduled to begin in the immediate future.

The Lumonics TEA laser to be used in the program was originally a Model 103 CO_2 laser. Conversion of the unit to a Model 203 HF/DF system has been completed by Lumonics Research, Ltd., and the laser is ready for operation at ARI.

The design of the aerosol handling system is complete. Work is well underway on the extensive plumbing required to carry the aerosol from a point ten feet above the roof of the building into the laboratory. An access hole in the roof has been constructed, and the ducting is being assembled. Completion is anticipated before the end of the calendar year. This includes the meteorological instrumentation described previously.

Thus, the major fabrication and assembly for the program should be completed by the end of 1974. The only exception to this will be the integration of the White cell into the system.

A milestone chart outlining the anticipated schedule over the next reporting period is shown in Figure 2.12. Alignment and preliminary calibration will occupy the better part of the first three months of 1975. It is anticipated that calibrated measurements of the aerosol scattering will begin by March 1974. Because of the late delivery of the White cell, calibrated extinction measurements will not begin until a month later. At that point, the first of April 1975, the aerosol characterization instrumentation and chemical analysis program will have been assembled and initial analyses performed. Consequently, by April 1975, it is anticipated that data acquisition will begin for simultaneous scattering and extinction using atmospheric aerosols.

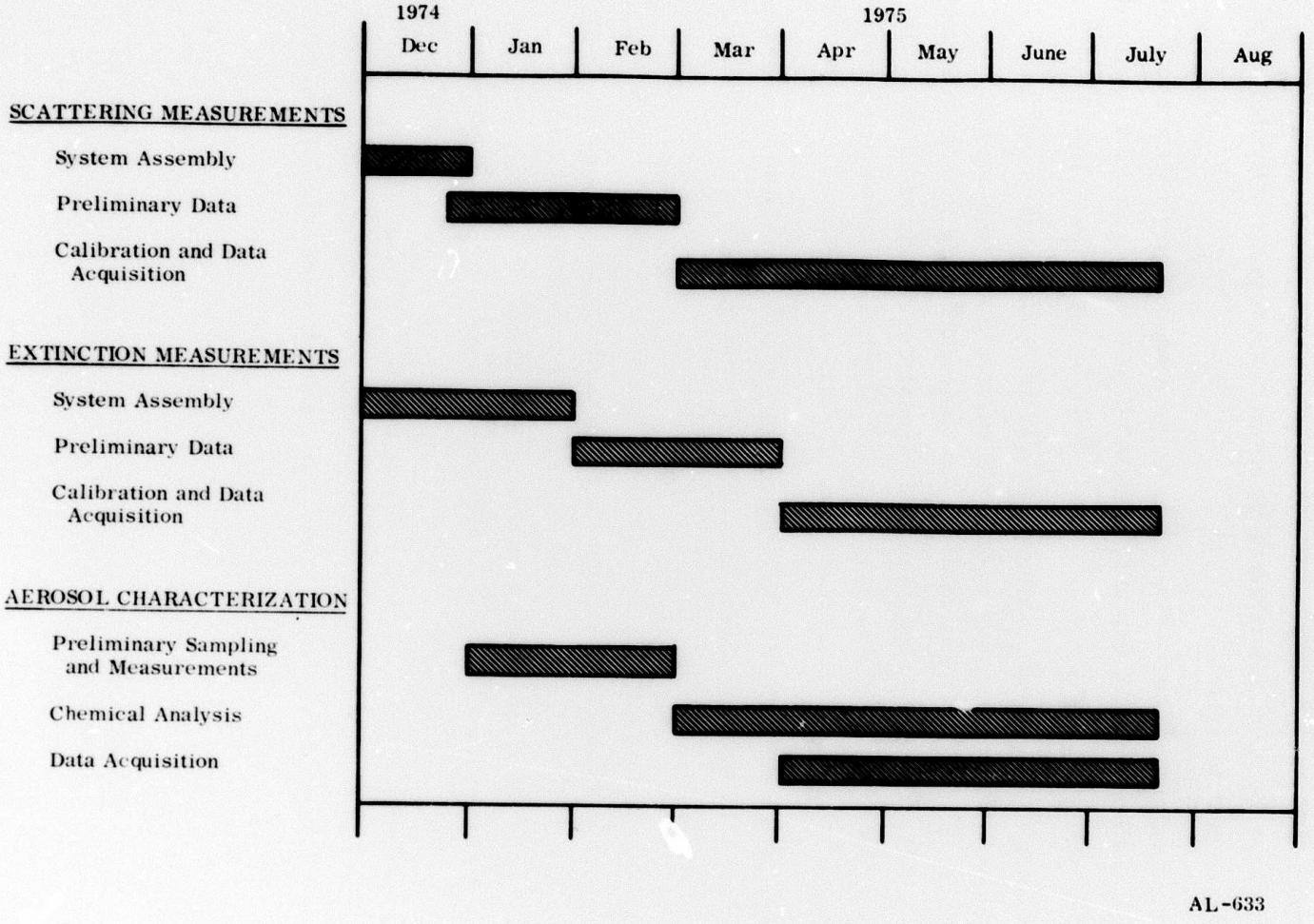

Figure 2.12 - Program Plan.

REFERENCES

1. T.H. Edwards, "Multiple-Traverse Absorption Cell Design," J. Opt. Soc. Am. 51, 98 (1961).

2. T.R. Ressor, "The Astigmatism of a Multiple Path Absorption Cell," J. Opt. Soc. Am. 41, 1959 (1951).

3. D.J. Speneer, "Atmospherie Gas Absorption at DF Laser Wavelengths," Proe. of the Meeting on Absorption of Infrared Laser Radiation in the Atmosphere, Mitre Corp., April 4 and 5, 1973.

4. L.D. Gray Young, " Relative Intensity Caleulations for Nitrous Oxide," J. Quant. Spectrosc. Rad. Transfer, 12 307 (1972).

5. S.K. Friedlander, "Chemical Element Balances and Identifieation of Air Pollution Sources," Environ. Sei. Tech. 7, 235 (1973).

6. E.S. Gladney, W.H. Zoller, A.G. Jones and G.E. Gordon, "Composition and Size Distributions of Atmospherie Particulate Matter in the Boston Area," Environ. Sci. Teeh., 8, 551 (1974).

MISSION
of
Rome Air Development Center

RADC is the principal AFSC organization charged with planning and executing the USAF exploratory and advanced development programs for information sciences, intelligence, command, control and communications technology, products and services oriented to the needs of the USAF. Primary RADC mission areas are communications, electromagnetic guidance and control, surveillance of ground and aerospace objects, intelligence data collection and handling, information system technology, and electronic reliability, maintainability and compatibility. RADC has mission responsibility as assigned by AFSC for demonstration and acquisition of selected subsystems and systems in the intelligence, mapping, charting, command, control and communications areas.